Panchromatic Ternary Organic Solar Cells with Porphyrin Dimers and Absorption-Complementary Benzodithiophene-based Small Molecules

Piradi, Venkatesh; Xu, Xiaopeng; Wang, Zaiyu; Ali, Jazib; Peng, Qiang; Liu, Feng; Zhu, Xunjin

Published in:
ACS Applied Materials and Interfaces

DOI:
10.1021/acsami.8b19240

Published: 13/02/2019

Document Version:
Peer reviewed version

ACS APPLIED MATERIALS & INTERFACES

Organic Electronic Devices

Panchromatic ternary organic solar cells with porphyrin dimers and absorption-complementary benzodithiophene-based small molecule

Venkatesh Piradi, Xiaopeng Xu, Zaiyu Wang, Jazib Ali, Qiang Peng, Feng Liu, and Xunjin Zhu

ACS Appl. Mater. Interfaces, **Just Accepted Manuscript** • DOI: 10.1021/acsami.8b19240 • Publication Date (Web): 18 Jan 2019

Just Accepted

ACS Publications

is published by the American Chemical Society. 1155 Sixteenth Street N.W., Washington, DC 20036

Panchromatic ternary organic solar cells with porphyrin dimers and absorption-complementary benzodithiophene-based small molecule

Venkatesh Piradi,[a]‡ Xiaopeng Xu,[b]‡ Zaiyu Wang,[c] Jazib Ali,[c] Qiang Peng,[b,] Feng Liu,[c,]* Xunjin Zhu,[a,]**

[a] *Institute of Molecular Functional Materials, Department of Chemistry and Institute of Advanced Materials, Hong Kong Baptist University, Waterloo Road, Kowloon Tong, Hong Kong, P. R.China. Email:xjzhu@hkbu.edu.hk*

[b] *Department of Chemistry, Sichuan University, Chengdu, Sichuan 610000, P. R. China. Email: qiangpeng@scu.edu.cn*

[c] *Department of Physics and Astronomy, and Collaborative Innovation Center of IFSA, Shanghai Jiao Tong University, Shanghai, 200240, P. R. China. E-mail: fengliu82@sjtu.edu.cn*

**Corresponding authors*

* xjzhu@hkbu.edu.hk (X. Z.); qiangpeng@scu.edu.cn (Q. P.); fengliu82@sjtu.edu.cn (F. L.).

KEYWORDS

Porphyrin dimers, diketopyrrolopyrrole, absorption-complementary, panchromatic, ternary organic solar cells

ABSTRACT

Diketopyrrolopyrrole-ethynylene-bridged porphyrin dimers are capped with electron deficient 3-ethylrhodanine (A_2) *via* a π-bridge of phenylene ethynylene, affording two new acceptor-donor-acceptor structural porphyrin dimers (DPP-2TTP and DPP-2TP) with strong absorption in ranges of 400–550 (Soret bands) and 700–900 nm (Q bands). Their intrinsic absorption deficiency between the Soret and Q bands could be perfect compensated by a wide bandgap small molecule DR3TBDTTF (D*) with absorption in 500–700 nm. Impressively, the optimal ternary device based on the blend films of DPP-2TPP, DR3TBDTTF (20 wt.%) and $PC_{71}BM$, shows a PCE of 11.15%, while the binary devices based on DPP-2TTP/$PC_{71}BM$ and DPP-2TP/$PC_{71}BM$ blend films exhibit PCEs of 9.30% and 8.23%, respectively. The high compatibility of the low bandgap porphyrin dimers with the wide bandgap small molecule provides a new threesome with $PC_{71}BM$ for highly efficient panchromatic ternary organic solar cells.

Introduction

Solution processed organic solar cells (OSCs), as an extensive green technology for solar energy production due to their potential mass production flexibility,[1-5] low cost fabrication of large area and lightweight devices by solution processing techniques.[6-12] In the past decade, the power conversion efficiency (PCE) has improved gradually to 14% for fullerene and non-fullerene based systems,[13-17] which can be either small molecule and polymer binary or ternary bulk heterojunction (BHJ) OSCs.[18-23] Although tandem OSCs containing two or more organic solar cells with different absorption maximum and width was reported with a record efficiency of 17%.[24-26] Whereas, ternary OSCs should be an advisable way to achieve notable PCE, which contain either three or more components (two donors and one acceptor or two acceptors and one donor system) in the active layer. Accordingly, a record efficiency of 14% has been achieved in ternary OSCs with significantly enhanced photon harvesting by using absorption or energy level complementary materials as the second donor or acceptor.[26] Most of the reported ternary OSCs are dominated by polymer donors or acceptors, whereas small molecules ternary devices have been sporadically reported.[27-31] Fabricating small molecule ternary devices play an essential contribution such as remarkable molecular design, synthesis, easy purification and no batch-to-batch variations.[32-35] Nian et al. reported recently, for ternary OSCs containing two molecule donors and an acceptor device exhibited PCE of 11%.[36] Previously, we and several other groups have continuously developed series of porphyrin small molecules as electron donors in OSCs with PCEs up to 10%.[37-44] Porphyrin derivatives are characteristic of strong absorption in a range of 400–500 nm (Soret band) and 550–650 nm (Q bands), whereas there is a very weak absorption between the Soret and Q bands. Structural modification by extending the π-conjugation with push-pull configuration only shifted the Soret and Q bands to longer wavelength range, but could not compensate the absorption

deficiency between them. For example, we ever reported a porphyrin dimer with strong absorption in ranges of 450–550 nm and 650–900 nm, but still weak absorption in a range of 550–650 nm.[45] Although its device performance in binary OSCs is not so impressive with PCE of 8.29%, its strong absorption in the short wavelength and deep near-infrared region render the porphyrin dimer an ideal donor component in small molecules ternary OSCs.[46] Particularly, a large pool of small molecules for highly efficient binary OSCs have been founded previously by chemists which could facilely provide an appropriate one with complementary absorption in the range of 550–650 nm.

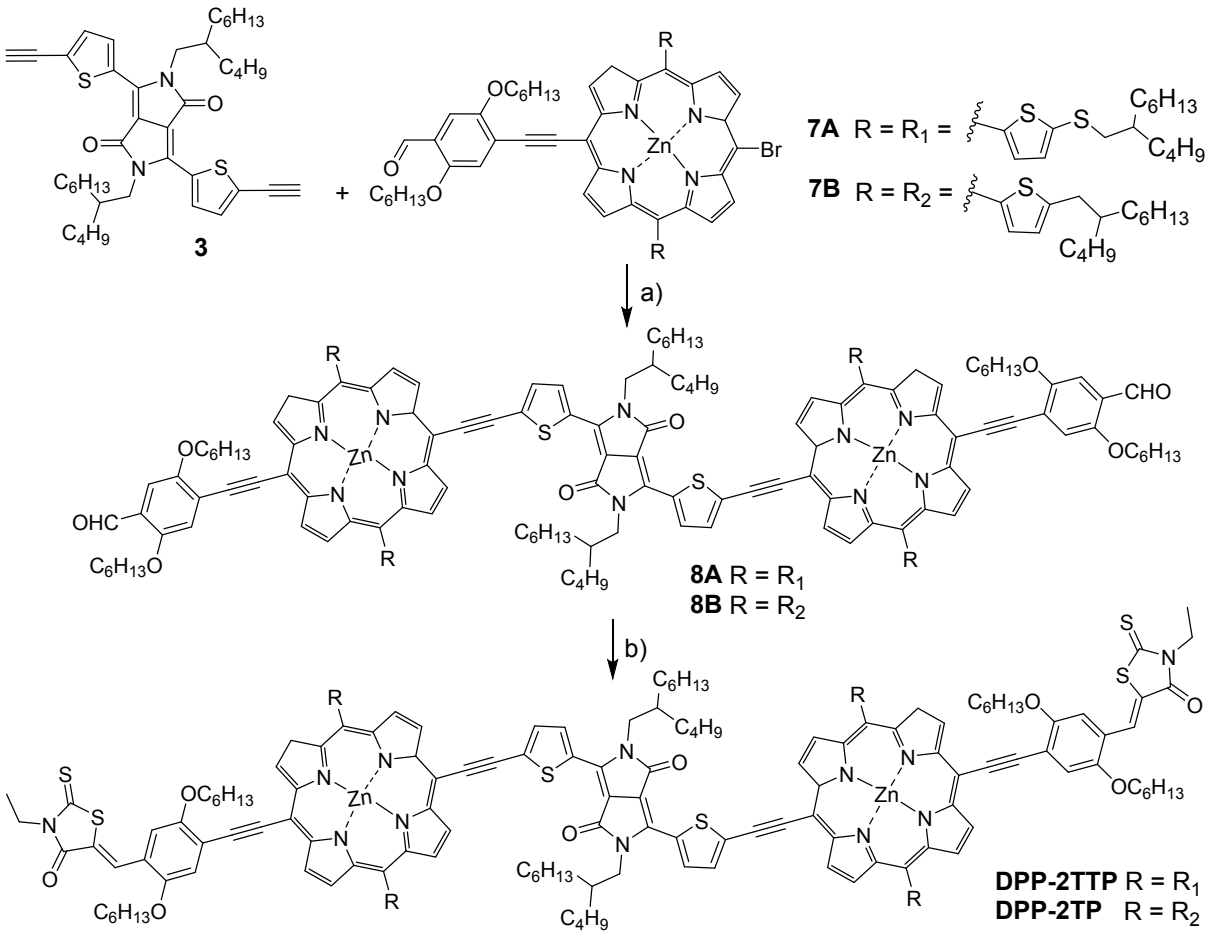

Scheme 1. Synthetic routes for DPP-2TTP and DPP-2TP. Reactions conditions: a) CuI, $Pd(PPh_3)_4$, THF, trimethylamine; b) 3-ethylrhodanine, dry $CHCl_3$, piperidine, reflux, overnight.

In this work, we synthesized two porphyrin dimers of DPP-2TTP and DPP-2TP (**Scheme 1**) with an optimal A_2-π-D-A_1-D-π-A_2 architecture, in which the two electron rich porphyrin units (D) were bridged by an electron deficient diketopyrrolopyrole (DPP) (A_1), endcapped with electron deficient 3-ethylrhodanine (A_2) *via* a π-bridge of phenylene ethynylene. The DPP-2TTP and DPP-2TP differ in the porphyrin units with alkylthiothiophene (TT) and alkylthiophene (T) as vertical *meso*-substitutions, respectively.[47] As expected, the two porphyrin dimers exhibited a very strong absorption in ranges of 400–550 nm (Soret bands) and 700-900 nm (Q bands), whereas the weak absorption between the Soret and Q bands could be perfect compensated by a wide bandgap small molecule of DR3TBDTTF with absorption in a range of 550–650 nm.[48] Subsequently, the two porphyrin dimers were used as electron donors with $PC_{71}BM$ as electron acceptor in binary OSCs, resulting in impressive device performances with PCEs up to 9.30%. Next, using absorption and energy level complementary small molecule DR3TBDTTF at a weight ratio of 20% as the second donor, the ternary device based on DPP-2TTP:20%DR3TBDTTF: $PC_{71}BM$ active layer showed a high PCE of 11.15 %, which was mainly ascribed to the enhanced photocurrent generation and high compatibility of the three components with an appropriate morphology.

Results and discussion

The synthetic routes of the intermediates of 1 2, 3, (4–8)A and (4–8)B and the targeting porphyrin dimers of DPP-2TTP and DPP-2TP are depicted in **Scheme S1** and **Scheme 1** with the details in Supporting Information (SI). The key intermediate 3, 7A, and 7B and were prepared according to the modified methods in literatures.[45, 49] Then the Sonogashira coupling of 7A and 7B with 3 led to the precursor 8A and 8B, respectively. The subsequent Knoevenagel condensation of 8A and 8B with 3-ethylrhodanine, respectively, afforded the porphyrin dimers of DPP-2TTP and DPP-2TP in good yields. Both the DPP-2TTP and DPP-2TP are soluble in most organic solvents for solution-processed BHJ OSCs.

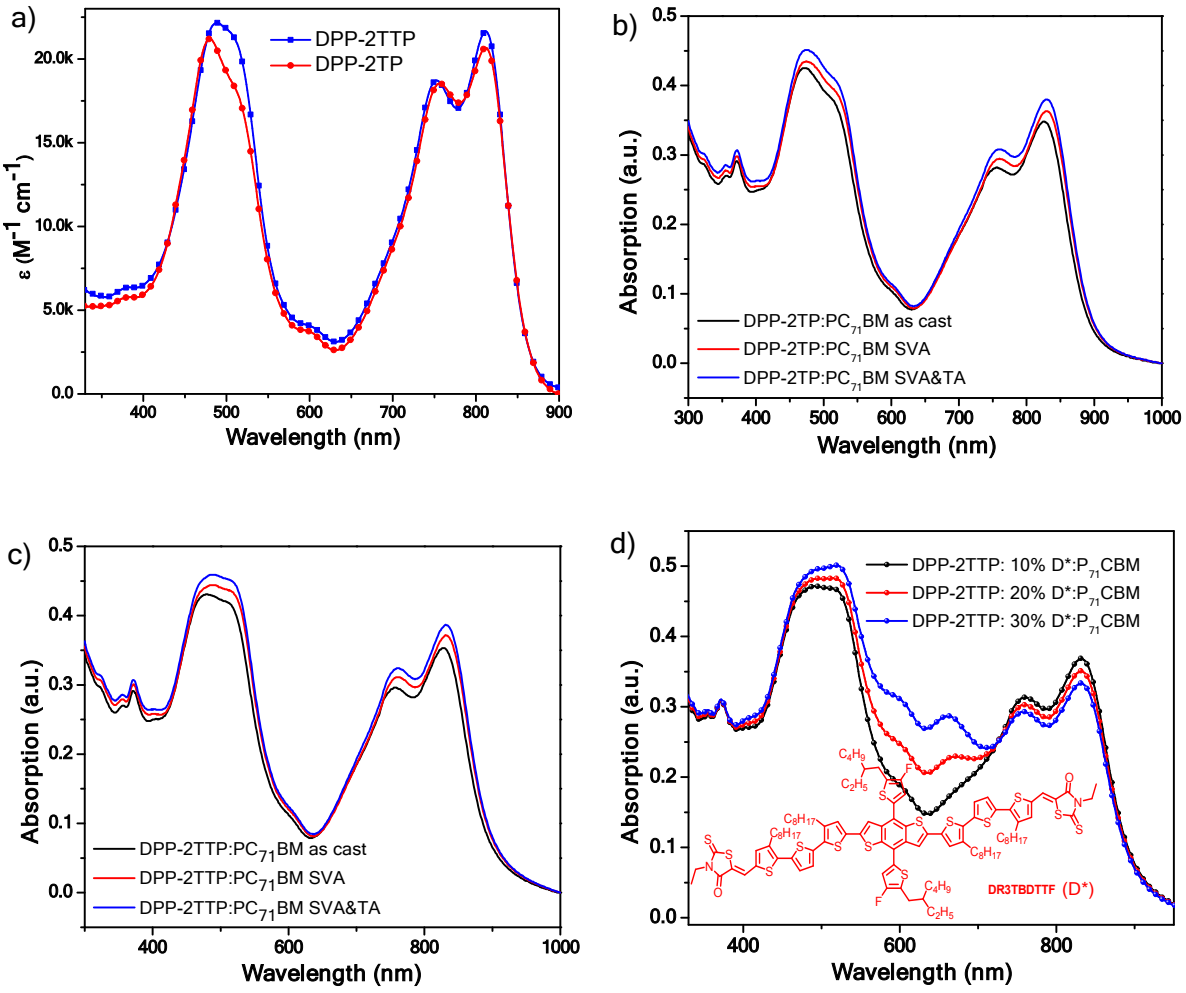

Figure 1. a) UV–vis-NIR absorption spectra of DPP-2TTP and DPP-2TP in chloroform solution ($1x10^{-5}$ M), absorption spectra of DPP-2TTP (b) and DPP-2TP (c) in films, d) DPP-2TTP: xD* (x = 10%, 20%, and 30%): $PC_{71}BM$ in films (insert: molecular structure of DR3TBDTTF).

The absorption spectra of DPP-2TTP and DPP-2TP were recorded in $CHCl_3$ solution. As shown in **Figure 1**a and compiled in **Table 1**, the broad and intense Soret band appears at 490 nm with molar extinction coefficient (ε) of $2.21 \times 10^5\ M^{-1}\ cm^{-1}$ for DPP-2TTP and 480 nm with ε of $2.1 \times 10^5\ M^{-1}\ cm^{-1}$ for DPP-2TP. The Q band attributes in the near-infrared region, which is 810 nm ($\varepsilon = 2.16 \times 10^5\ M^{-1}\ cm^{-1}$) with a weak shoulder of 762 nm for DPP-2TTP, similarly, 812 nm ($\varepsilon = 2.04 \times 10^5\ M^{-1}\ cm^{-1}$) and 760 nm with for DPP-2TP. The wide and near-infrared absorption

of Q bands from 650 to 870 nm is ascribed to the efficient conjugation of the backbone structure of porphyrin dimer and intramolecular charge transfer (ICT) between the terminal acceptor units through the π-linker.[50-52] The blend thin films DPP-2TTP (or DPP-2TP): $PC_{71}BM$ (1:1.5, w/w) were spin-coated from their chlorobenzene (CB) solutions and processed under solvent-vapor annealing (SVA) and thermal annealing (TA). The film spectra as shown in **Figure 1**(b, c) disclose significantly broad bathochromic absorption extended into NIR region over 1000 nm, which indicates stronger interelectronic π-π aggregations between the porphyrin dimers in the film. In addition, those films under SVA and TA processing show slightly increased intensity of absorption due to more orderly packed molecular interactions.[53] Next, the blend films of DR3TBDTTF (D*) at a weight ratio of 10, 20, and 30%, respectively, with DPP-2TTP and $PC_{71}BM$ (DPP-2TTP:xD*:PCBM, x = 10%, 20%, and 30%) were prepared similarly and recorded with full spectra in the visible-NIR region from 300 to1000 nm (**Figure 1**d) because of the significant contribution of DR3TBDTTF component in a range of 550–700 nm. Moreover, the optical band gaps (E_g^{opt}) were measured from the onset wavelength (λ_{onset}) of the absorption spectra of solution using E_g^{opt} =1240 / λ_{onset} (eV), with low band gap values of 1.33 for DPP-2TTP and 1.34 eV for DPP-2TP.

Table 1. Photophysical and electrochemical properties of DPP-2TTP and DPP-2TP

Comp	λ_{max}/nm ($\varepsilon/10^5 M^{-1}cm^{-1}$)	λ_{max}/nm (Film)	λ_{onset}/nm (Solution)	E_{ox} [V]	E_{HOMO} (eV)	E_{LUMO} (eV)	Eg (eV)
DPP-2TTP	490 (2.21), 752 (1.86), 810 (2.16)	485, 762, 831	932	0.38	−5.18	−3.77	1.33
DPP-2TP	480 (2.10), 755 (1.86), 812 (2.04)	475, 760, 830	923	0.36	−5.16	−3.76	1.34

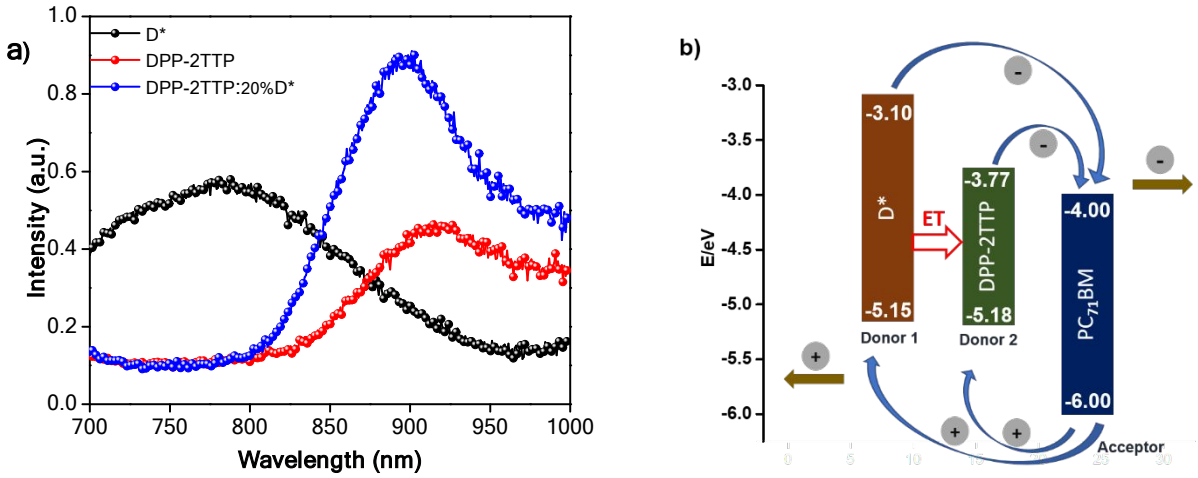

Figure 2. a) PL spectra (excited at 660 nm) of pristine films of D*, DPP-2TTP and the binary blend film of DPP-2TTP: 20%D*; b) The energy diagram of D*, DPP-2TTP and $PC_{71}BM$.

Photoluminescence (PL) were performed to study the charge transfer process for the blend films. **Figure 2** (a) shows the PL spectra of the pristine and the binary blend films of D* and DPP-2TTP. When excited at 660 nm in an overlap absorption region of DPP-2TTP and D*, both the pristine films of D* and DPP-2TTP exhibits weak PL in the near-infrared region, whereas the blend film DPP-2TTP:20%D* exhibits a quenched PL of D* and intensity increased PL of DPP-2TTP. The result indicates efficient energy transfer (ET) from D* to DPP-2TTP, which is also supported by the large overlap between the emission spectrum of D* and the absorption spectrum of DPP-2TTP. Obviously, the efficient energy transfer between the two components is helpful to achieve high photocurrent in ternary OSCs. At the same time, the efficient energy transfer implies a good miscibility between D* and DPP-2TTP molecules, which is conducive to the formation of appropriate phase separation for high fill factor (FF) in ternary OSCs.[54] Their sequential alignment of highest occupied molecular orbitals (HOMOs) and lowest unoccupied molecular orbitals (LUMOs) (**Figure 2**b), also depicts that excitons could be efficient generated after light irradiation

and undergo a considerable charge separation and transfer at the ternary blend interface of DPP-2TTP:D*:$PC_{71}BM$.[55]

Cyclic voltammetry (CV) of two porphyrin dimers were recorded in $CHCl_3$ solution to estimate the energy levels and study the redox properties. As shown in **Figure S1** (SI) and **Table 1**, the highest occupied molecular orbital (HOMO) energy levels were calculated from the onset of oxidation peaks to be −5.18 and −5.16 eV, and the corresponding lowest unoccupied molecular orbitals (LUMOs) were estimated to be −3.77 and −3.76 eV ($E_{LUMO} = E_{HOMO} + E_g$) for DPP-2TTP and DPP-2TP, respectively. The introduction of sulfur atoms in alkyl chains for DPP-2TTP does not effect on the band gap but slightly lowers its HOMO level due to the unique electron donating property of sulfur atom, which would lead to higher V_{OC} (*vide infra*).[56] For consistence, the CV of D* was also recoded under the same conditions and its HOMO/LUMO energy levels were calculated to be −5.15/−3.10. As shown in **Figure 2**d, the perfect sequential alignment of their HOMO/LUMO energy levels indicated the electron at their interfaces could efficiently transfer from DR3TBDTTF (D*) to DPP-2TTP and then $PC_{71}BM$ for the descending order of LUMOs, while hole transfers reversibly for the increasing order of HOMOs. In other words, DPP-2TTP might act as electron and hole transfer relay between the DR3TBDTTF and $PC_{71}BM$.

The photovoltaic studies were performed using DPP-2TTP and DPP-2TP as donors in the binary devices of ITO/PEDOT:PSS/Donor:$PC_{71}BM$/ZrAcac/Al under the simulated AM 1.5 G illumination at 100 mW cm^{-2}. After the systematic optimization (see **Table S1**, **S2**, and **Figure S2** in SI), the optimal devices were screened out with a combination of chlorobenzene (CB): pyridine:1,8-diiodooctane (DIO) at 96:3:1 volume ratio (v%) and thermal annealing at 100 ^{o}C for 10 mins. The photovoltaic parameters of the optimal binary devices were summarized in **Table 2**. And the corresponding current density versus voltage (*J-V*) characteristics and the external

quantum efficiency (EQE) curves were illustrated in **Figure 3** (a, b) respectvily. The optimal binary devices exhibit a maximum PCE of 9.30% with an open circuit voltage (V_{OC}) of 0.80 V, a short circuit current (J_{SC}) of 16.35 mA cm^{-2} and a fill factor (FF) of 71.1% for DPP-2TTP and similarly, a PCE of 8.23%, a V_{OC} of 0.76 V, a J_{SC} of 15.65 mA cm^{-2} and a FF of 69.2% for DPP-2TP. Impressively, the two binary systems gained reliable low photon energy loss (E_{loss}) of 0.58 eV for DPP-2TTP and 0.6 eV for DPP-2TP, which is essential for the enhancement of J_{sc} and PCE values. Peng *et al.* published DPP-porphyrin small molecule with a very low energy band gap of 1.37 eV and a high V_{oc} of 0.78 V was achieved in BHJ OSCs and followed by a low energy loss of 0.59 eV.[40] These results indicated a suitable alignment of the HOMO/LUMO energy levels of those components in the ternary blend active layer.

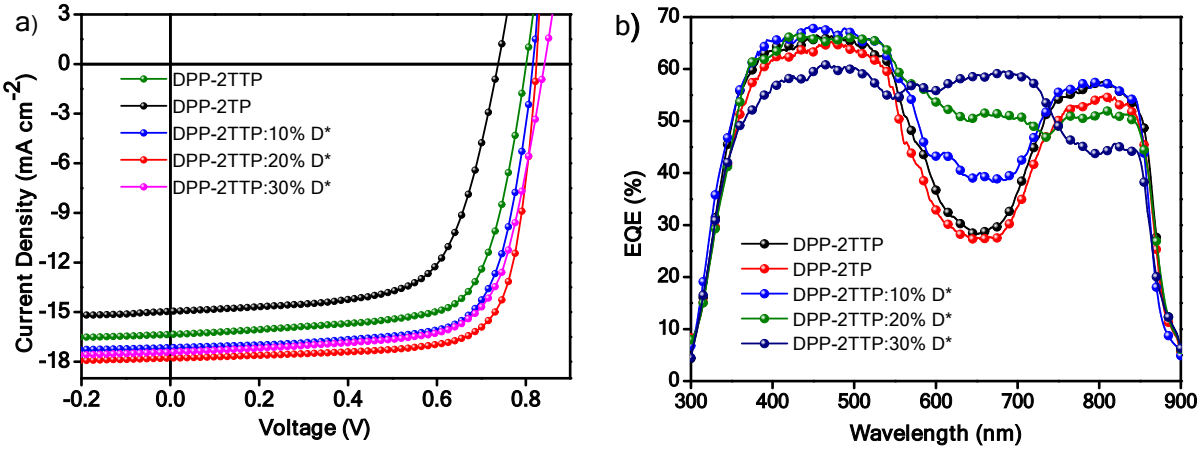

Figure 3. (a) Current density-voltage (*J-V*) curves and (b) the EQE curves for the devices under constant incident light intensity (AM 1.5G, 100 mW cm^{-2}) without and with SVA.

Table 2. Hole and electron mobilities and key parameters of device performances[a]

Device	J_{SC} (mA cm^{-2})	V_{OC} (V)	FF (%)	PCE (%)[b]	μ_h (cm^2/Vs)	μ_e (cm^2/Vs)	μ_e/μ_h
DPP-2TTP: $PC_{71}BM$	16.35 ± 0.08 (16.02)[b]	0.80 ± 0.01	71.1 ± 0.3	9.10 ± 0.20	1.25×10^{-4}	8.16×10^{-5}	0.65

DPP-2TP: $PC_{71}BM$	15.54 ± 0.09 (15.21)	0.76 ± 0.01	68.7 ± 0.3	8.00 ± 0.11	8.83×10^{-5}	4.32×10^{-5}	0.49
DPP-2TTP: 10%D*:$PC_{71}BM$	17.16 ± 0.13 (16.93)	0.81 ± 0.02	73.3 ± 0.1	10.03 ± 0.16	1.72×10^{-4}	1.28×10^{-4}	0.74
DPP-2TTP: 20%D*:$PC_{71}BM$	17.78 ± 0.11 (17.61)	0.82 ± 0.03	76.5 ± 0.6	11.01 ± 0.14	3.21×10^{-4}	2.84×10^{-4}	0.88
DPP-2TTP: 30%D*:$PC_{71}BM$	17.41 ± 0.19 (17.22)	0.83 ± 0.06	71.6 ± 0.2	10.16 ± 0.18	2.36×10^{-4}	1.97×10^{-4}	0.83

[a] Each value is averaged from 8 devices with standard deviation after ±. [b] Values in brackets are calculated from EQE.

Although the optimal binary devices showed a wide photocurrent response extending into 900 nm owing to the contribution of low bandgap porphyrin-based small molecules, the low EQE value of 27% at the bottom of the valley clearly reflected the intrinsic absorption deficiency between the Soret and Q bands in porphyrin-based small molecules. It is believed that ternary OSCs containing one more donor or acceptor have great potential to reduce the energy loss, enhance light-harvesting capability and improve device performance. Therefore, the wide bandgap small molecule electron donor DR3TBDTTF was selected as a third component for ternary OSCs for its complementary absorption spectrum and aligned energy levels regarding porphyrin-based small molecules. The blend films were fabricated from DPP-2TTP:D*:$PC_{71}BM$ with different weight ratio (w/w) of D* at 10%, 20%, and 30% in 0.3 volume% of pyridine and chlorobenzene solution. Compared with the binary device DPP-2TTP: $PC_{71}BM$, the ternary devices based on the three active layers DPP-2TTP:xD*:$PC_{71}BM$ (x = 10%, 20%, 30%, w/w) exhibit enhanced PCEs of 10.19%, 11.15% and 10.34% respectively. And the current density-voltage (*J-V*) characteristics are displayed in **Figure 3**a. For the ternary, the content of D* increased from 10 to 20 wt.%, led to progressively enhanced J_{SC} from 17.29 to 17.89 mA cm^{-2}, FF from 73.4 to 77.1% 76.5%, and V_{OC} from 0.83 to 0.85 V. This is mainly due to the improved light-harvesting capability in the range of 550–700 nm and favorable morphology for efficient charge dissociation and transfer in ternary devices with D*,

which is well consistent with PL experiments. Further increasing the content of DR3TBDTTF could continue to improve the light-harvesting in the range of 550–700 nm, but impair the light-harvesting in the Soret and Q regions of porphyrin-based small molecules. At the same time, high content of D* would lead to unfavorable morphology. As a result, the ternary device with 30% DR3TBDTTF exhibits a balanced J_{SC}, slightly enhanced V_{OC}, but significantly decreased FF, as a whole an inferior PCE of 10.34%. In addition, the integrated J_{SC} values are listed in **Table 2** from EQE spectra for all the devices are consistent with *J–V* measurements with errors in 2%).

Further, we studied the exciton generation, dissociation and charge collection of the active layers through the charge photocurrent density (J_{sat}) and the effective voltage (V_{eff}). The binary DPP-2TTP:$PC_{71}BM$, DPP-2TP:$PC_{71}BM$ and optimized ternary DPP-2TTP:20%D*:$PC_{71}BM$ devices were carried under SVA conditions as shown in **Figure S3**a (SI). The photocurrent density (J_{ph}), as a function of the $V_{eff} = V_0 - V_a$, where V_0 is voltage when $J_{ph} = 0$ and V_a is the applied voltage, is calculated by $J_{ph} = J_L - J_D$, where J_L is the current density under illumination and J_D is the current density in the dark.[57, 58] Obviously, the J_{ph} increases rapidly with the increasing voltages within lower levels and becomes saturated when the effective voltage V_{eff} reaches 0.34 V, 0.32 V and 0.38 V for the devices based on the active layers of DPP-2TTP, DPP-2TP and DPP-2TTP:20%D*, respectively, which means that all the photo-generated excitons would be dissociated to free charge carriers and collected by the electrodes under high internal electric field. Moreover, the charge dissociation probabilities P(*E,T*) was conducted by normalizing of J_{ph} with J_{sat} under short circuit condition (J_{ph}/J_{sat}) to be 0.92% for DPP-2TTP: $PC_{71}BM$, 0.93% for DPP-2TP:$PC_{71}BM$ and 0.95% for DPP-2TTP:20%D*:$PC_{71}BM$, as shown in **Figure S3**a . The higher P(*E,T*) value for ternary blend was correlated to the excellent J_{SC} of 17.78 mA cm^{-2}, suggesting

that the contribution of 20% D* to the ternary blend is more capable for efficient charge collection than the binary devices.[57, 59-61]

To get more information about the effect of the involvement of D* on the charge recombination dynamics of the ternary devices, the variations of J_{SC} and V_{OC} versus light intensity were evaluated, respectively. As shown in **Figure S3** (b, c) (SI) the slope (α) of the ternary device was calculated to be 0.997 for DPP-2TTP:20%D*, which is slightly higher than that of the binary devices with values of 0.991 and 0.981 for DPP-2TTP and DPP-2TP, respectively. The α values close to 1 (α < 1) implies that bimolecular recombination is not a crucial loss mechanism in both binary and ternary devices. On the other hand, the slope ($S = kT/q$, where k is Boltzmann's constant, T is the temperature and q is the elementary charge) of the V_{OC} versus the natural logarithm of the light intensity, were predicted to be 1.19 (kT/q) for DPP-2TTP and 1.27 (kT/q) for DPP-2TP of the binary devices. As expected, the ternary blend of DPP-2TTP: 20%D* shows a lower slope of 1.10 (kT/q), implying a reduced trap-assisted recombination. As a result, the ternary device shows the highest FF of 76.5% and V_{OC} of 0.85 V.[62]

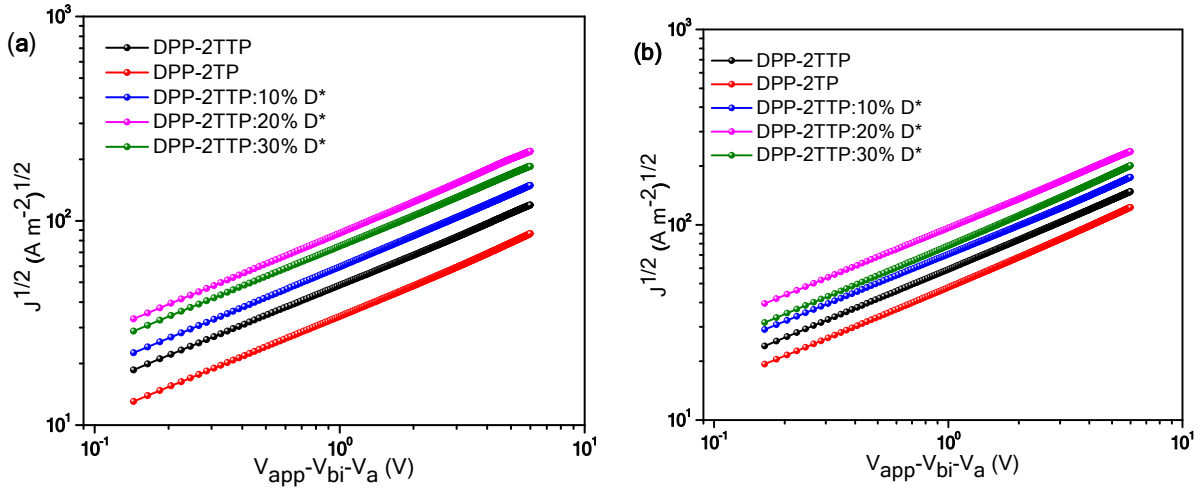

Figure 4. Dark current-voltage characteristics of a) hole and b) electron only devices based on optimized devices Glass/ITO/PEDOT: PSS/active layer/MoO_3/Au and glass/Al/active layer/Al.

To further investigate the effect of D* on the performance of ternary solar cells, hole and electron mobilities of the optimal devices ITO/PEDOT: PSS/active layer/MoO_3/Au were measured by space charge limited current (SCLC) method as shown in **Figure 4** (a, b) and the estimated values are displayed in **Table 2**. The hole mobilities of the binary films were calculated to be 1.25×10^{-4} and cm^2/Vs for DPP-2TTP: $PC_{71}BM$, 8.83×10^{-5} cm^2/Vs for DPP-2TP: $PC_{71}BM$, and 1.72×10^{-4}, 3.21×10^{-4} and 2.36×10^{-4} cm^2/Vs for the DPP-2TTP:xD*:$PC_{71}BM$ (x = 10, 20, 30%), respectively. The electron mobilities are noted to be 8.16×10^{-5} cm^2/Vs for DPP-2TTP:$PC_{71}BM$, 4.32×10^{-5} cm^2/Vs for DPP-2TP:$PC_{71}BM$, and 1.28×10^{-4}, 2.84×10^{-4} and 1.97×10^{-4} cm^2/Vs for the DPP-2TTP:xD*:$PC_{71}BM$ (x = 10, 20, 30%), respectively. The hole and electron mobilities were increased dramatically with the 20% weight ratio of D* in the ternary blend and then decreased with 30% of D*, this clearly suggesting that molecular arrangement could be adjusted by the contribution of D*. Moreover, electron to hole (μ_e/μ_h) ratio of DPP-2TTP:20%D*:$PC_{71}BM$ shows a notable value of 0.88, which means the charge transport is more balanced on the 20% weight ratio of D* in the blend film. This process is applicable to increase the crystallinity and nanoscale morphology of the active layers. Whereas, the ternary blend of D* (30%) dropped from 0.88 to 0.83, which led to unbalanced hole and electron mobilities due to unfavorable morphology.

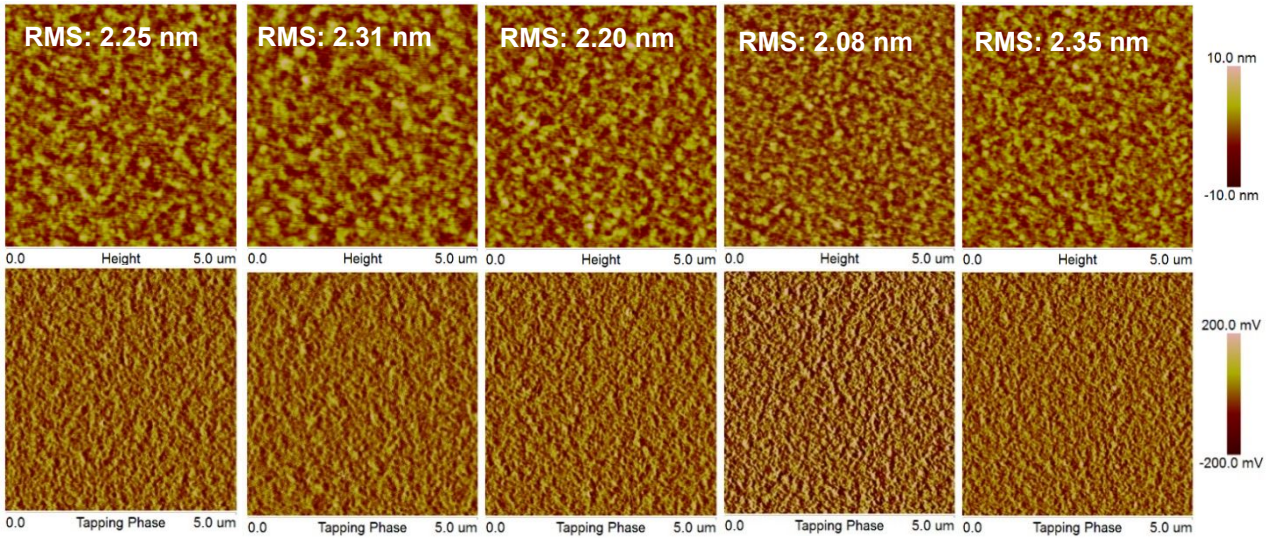

Figure 5. AFM height images (top) and phase images (bottom) of binary blend films of DPP-2TTP:$PC_{71}BM$, DPP-2TP:$PC_{71}BM$ and ternary blend films of DPP-2TTP:xD*:$PC_{71}BM$ (x = 10%, 20%, 30%) from left to right. The scan size is 5 μm × 5 μm for all images.

At the same time, the morphology of the optimized binary and ternary blend films was analyzed by trapping-mode atomic force microscopy (AFM). As shown in **Figure 5**, the height images (top) from the corresponding binary devices DPP-2TTP:$PC_{71}BM$, DPP-2TP):$PC_{71}BM$ and DPP-2TTP:xD*:$PC_{71}BM$ (x = 10%, 20%, 30%) are correlated to a root mean square roughness (RMS) of 2.25 nm, 2.31 nm, 2.20 nm, 2.08 nm, and 2.35 nm, respectively. Obviously, a smoother surface with an RMS of 2.08 nm was observed with 20% D* in the ternary blend, which should be beneficial for more efficient exciton dissociation and charge transport to support for higher J_{sc} and PCE values. On the contrary, the doping of 30% D* led to unfavorable morphology with larger phase separation. On the other side, the phase images (bottom) also indicate that the 20%D* in the ternary blend is helpful to form bicontinuous interpenetrated heterojunction structure for efficient charge dissociation and transfer.

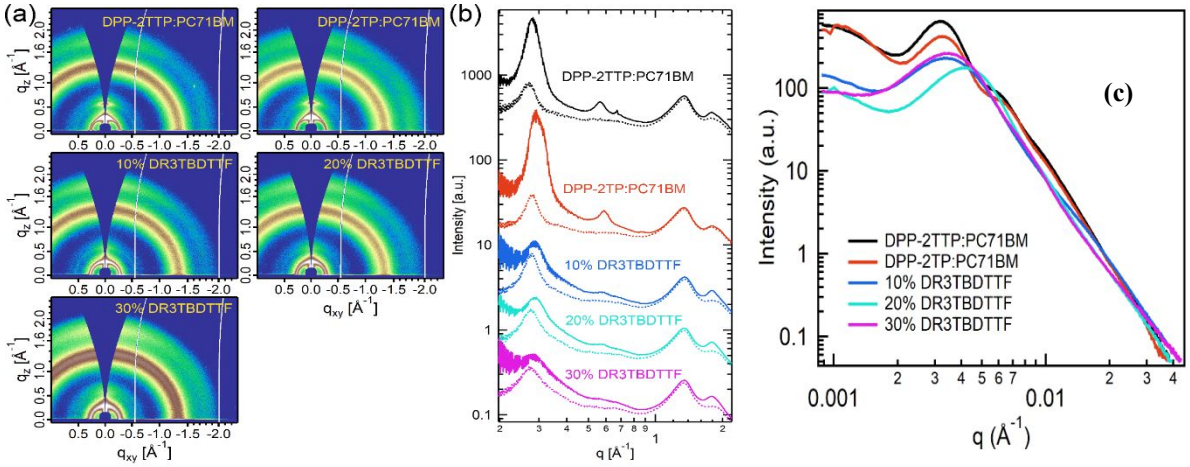

Figure 6. a) GIWAXS 2D diffraction patterns, b) out-of-plane (solid line) and in-plane (dotted line) line-cut profiles, and c) RSoXS profiles of DPP-2TTP:$PC_{71}BM$, DPP-2TP:$PC_{71}BM$ binary blend films and DPP-2TTP:xD*: $PC_{71}BM$ ternary blend films (x = 10%, 20% and 30%).

Detailed molecular packing information was acquired by performing grazing incidence wide-angle X-ray scattering (GIWAXS) measurements. The 2D GIWAXS patterns and corresponding out-of-plane and in-plane line-cuts are shown in **Figure 6** (a, b) When blending with $PC_{71}BM$ in binary systems, both DPP-2TTP and DPP-2TP show sharp (100) diffraction peaks in both in-plane and out-of-plane directions, with $q \sim 0.27$ Å^{-1} (d-spacing: 23.3 Å) for DPP-2TTP and $q \sim 0.28$ Å^{-1} (d-spacing: 22.4 Å) for DPP-2TP respectively. DPP-2TTP shows preferential face-on orientation with stronger out-of-plane (010) π-π stacking peak at $q \sim 1.78$ Å^{-1} (d-spacing: 3.53 Å), whereas DPP-2TP exhibits no preferential π-π stacking orientation judging from the almost isotropic scattering ring at $q \sim 1.78$ Å^{-1}. The coherence length of out-of-plane (010) π-π stacking peak was calculated to be 20.5 Å and 19.0 Å for DPP-2TTP and DPP-2TP respectively. Although DPP-2TP had a better lamellar packing than DPP-2TTP with a more pronounced (100) peak, preferential face-on π-π stacking of DPP-2TTP made it more beneficial for charge transport, which is shown in the enhancement of hole mobility and FF. When the third component D* was added to the DPP-2TTP:$PC_{71}BM$ blend, the lamellar packing of DPP-2TTP was greatly depressed as evidenced by weakening and broadening of the (100) peaks in both in-plane and out-of-plane directions. The coherence length of DPP-2TTP lamellar packing decreased from 12.8 nm in binary film to 12.5, 9.6 and 7.1 nm with addition of 10%, 20% and 30% D*. Similarly, the coherence length of π-π stacking also shrank slightly from 2.6 nm to 2.5, 2.2 and 2.1 nm. Considering that no D* diffraction peak was observed in the ternary blend films, we concluded that DR3TBDTTF dissolve into the DPP-2TTP domain and disturb the molecular packing of DPP-2TTP inhibiting formation of big crystallites. However, the increased integrated intensity of (100) and (010) diffraction peaks indicated that the crystallinity of donor domain in ternary systems was improved with the addition of D*, resulting in the enhanced mobility and FF of the devices.

Resonant soft X-ray scattering (RSoXS) was used to investigate the phase separation of binary and ternary blend films. A photon energy of 284.2 eV was selected to enhance the contrast between PCBM and donor blends. As seen from **Figure 6**c, both DPP-2TTP:$PC_{71}BM$ and DPP-2TP:$PC_{71}BM$ binary blend films showed similar scattering profiles with main peak located at $q \sim 0.0032$ $Å^{-1}$, corresponding to a phase separation distance of ~ 190 nm, and shoulder peak at high q which is caused by refined phase separation. There are also scattering peaks in the low q region beyond the detection limits, which means larger phase separation in binary blends as confirmed by the AFM results. The addition of D* attenuated the scattering peak in the low q and prevented the ternary blend films from forming larger phase separation which was detrimental for charge generation. Compared with the DPP-2TTP:$PC_{71}BM$ film, the prime peak shifted to ~ 0.0034, 0.0042 and 0.0035 $Å^{-1}$ with smaller phase separation distance of 184, 150 and 180 nm in the ternary blend films with (10%, 20%, 30%)D* respectively. Although the phase separation distance reduced in ternary films, such phase separation distance was still too large for efficient charge separation since exciton diffusion length is generally considered to be ~ 10 nm. This indication clearly showed hierarchical morphology containing smaller domains had formed in the blend film.

Conclusions

In summary, two low bandgap porphyrin-based small molecules DPP-2TTP and DPP-2TP have been prepared and showed an intrinsic absorption range 400–550 (Soret bands) and 700–900 nm (Q bands). To overcome the absorption deficiency from 550 to 700 nm, a wide bandgap small molecule DR3TBDTTF has been contributed and optimized for the ternary devices. Such a combination performed synergically to improve the absorption range over 1000 nm and the key parameters as well. Especially, the device based ternary blend DPP-2TPP:20% DR3TBDTTF:$PC_{71}BM$ showed a remarkable PCE of 11.15% with a significant FF of 77.1%,

which is highly considerable in comparison with the binary devices on DPP-2TTP:$PC_{71}BM$ (9.30%) and DPP-2TP:$PC_{71}BM$ (8.23%). The improved overall performance of the ternary devices could be attributed to complementary absorption of the two donors and favorable film morphology for the reduced recombination and enhanced charge extraction.

ASSOCIATED CONTENT

Supporting Information

The Supporting information is available free of charge on the http://pubs.acs.org/

The details of the synthesis and characterization of the targeting compounds DPP-2TTP and DPP-2TP, the intermediates 1–3, 4A–8A, and 4B–8B, device fabrication, photovoltaic performances and *J-V* curves under various conditions, Variation of J_{SC} and V_{OC} with illumination intensity, J_{ph}-V_{eff} characteristics, NMR spectra and MALDI-TOF mass spectra.

ACKNOWLEDGEMENTS

This work was supported by the Hong Kong Research Grants Council (HKBU 22304115-ECS and and C5015-15GF), Areas of Excellence Scheme ([AoE/P-03/08]), Hong Kong Baptist University (FRG2-16-17-024, FRG2-17-18-068), the Inter-institutional Collaborative Research Scheme (RC-ICRS/15-16/02E, RC-ICRS/1617/02C-CHE), and the Interdisciplinary Research Matching Scheme (RC-IRMS/16/17/02CHEM). Portions of this research were carried out at beamline 7.3.3 and 11.0.1.2 at the Advanced Light Source, and Molecular Foundry, Lawrence Berkeley National Laboratory, which was supported by the DOE, Office of Science, and Office of Basic Energy Sciences.

ABBREVIATIONS

Nucleur magnetic resonance (NMR), Matrix-assisted laser desorption/ionization-time-of-flight (MALDI-TOF)

AUTHOR INFORMATION

Corresponding Author

* (X. Z.) xjzhu@hkbu.edu.hk; (Q. P.) qiangpeng@scu.edu.cn; (F. L.) fengliu82@sjtu.edu.cn.

Author Contributions

‡These authors contributed equally.

Notes

The authors declare no competing financial interest.

REFERENCES

1. Darling, S. B.; You, F., The Case for Organic Photovoltaics. *RSC Adv.* **2013,** *3*, 17633-17648.

2. Li, G.; Shrotriya, V.; Huang, J.; Yao, Y.; Moriarty, T.; Emery, K.; Yang, Y., High-efficiency Solution Processable Polymer Photovoltaic Cells by Self-organization of Polymer Blends. In *Materials For Sustainable Energy: A Collection of Peer-Reviewed Research and Review Articles from Nature Publishing Group*, World Scientific: 2011; pp 80-84.

3. Liang, Y.; Xu, Z.; Xia, J.; Tsai, S. T.; Wu, Y.; Li, G.; Ray, C.; Yu, L., For the Bright Future—Bulk Heterojunction Polymer Solar Sells with Power Conversion Efficiency of 7.4%. *Adv. Mater.* **2010,** *22*, E135-E138.

4. Park, S. H.; Roy, A.; Beaupré, S.; Cho, S.; Coates, N.; Moon, J. S.; Moses, D.; Leclerc, M.; Lee, K.; Heeger, A. J., Bulk Heterojunction Solar Cells with Internal Quantum Efficiency Approaching 100%. *Nat. Photonics* **2009,** *3*, 297-302.

5. Yu, G.; Gao, J.; Hummelen, J. C.; Wudl, F.; Heeger, A. J., Polymer Photovoltaic

Cells: Enhanced Efficiencies via a Network of Internal Donor-Acceptor Heterojunctions. *Science* **1995,** *270*, 1789-1791.

6. Emmott, C. J.; Röhr, J. A.; Campoy-Quiles, M.; Kirchartz, T.; Urbina, A.; Ekins-Daukes, N. J.; Nelson, J., Organic Photovoltaic Greenhouses: A Unique Application for Semi-transparent PV? *Energy Environ. Sci.* **2015,** *8*, 1317-1328.

7. Krebs, F. C.; Espinosa, N.; Hösel, M.; Søndergaard, R. R.; Jørgensen, M., 25th Anniversary Article: Rise to Power–OPV-based Solar Parks. *Adv. Mater.* **2014,** *26*, 29-39.

8. Li, G.; Zhu, R.; Yang, Y., Polymer Solar Cells. *Nat. Photonics* **2012,** *6*, 153-161.

9. Po, R.; Bernardi, A.; Calabrese, A.; Carbonera, C.; Corso, G.; Pellegrino, A., From Lab to Fab: How Must the Polymer Solar Cell Materials Design Change?–An Industrial Perspective. *Energy Environ. Sci.* **2014,** *7*, 925-943.

10. Polman, A.; Knight, M.; Garnett, E. C.; Ehrler, B.; Sinke, W. C., Photovoltaic Materials: Present Efficiencies and Future Challenges. *Science* **2016,** *352*, 4424 (1-10).

11. Wright, M.; Uddin, A., Organic—Inorganic Hybrid Solar Cells: A Comparative Review. *Sol. Energy Mater. Sol. Cells* **2012,** *107*, 87-111.

12. Wu, J.-S.; Cheng, S.-W.; Cheng, Y.-J.; Hsu, C.-S., Donor–acceptor Conjugated Polymers based on Multifused Ladder-type Arenes for Organic Solar Cells. *Chem. Soc. Rev.* **2015,** *44*, 1113-1154.

13. Vartanian, M.; Singhal, R.; de la Cruz, P.; Biswas, S.; Sharma, G. D.; Langa, F., Low Energy Loss of 0.57 eV and High Efficiency of 8.80% in Porphyrin-based BHJ Solar Cells. *ACS Appl. Energy Mater.* **2018,** *1*, 1304-1315.

14. Li, M.; Gao, K.; Wan, X.; Zhang, Q.; Kan, B.; Xia, R.; Liu, F.; Yang, X.; Feng, H.; Ni, W., Solution-processed Organic Tandem Solar Cells with Power Conversion Efficiencies> 12%. *Nat. Photonics* **2017,** *11*, 85-90.

15. Wu, Y.; Li, Z.; Ma, W.; Huang, Y.; Huo, L.; Guo, X.; Zhang, M.; Ade, H.; Hou, J., PDT-S-T: A New Polymer with Optimized Molecular Conformation for Controlled Aggregation and π–π Stacking and Its Application in Efficient Photovoltaic Devices. *Adv. Mater.* **2013,** *25*, 3449-3455.

16. Zhao, W.; Li, S.; Yao, H.; Zhang, S.; Zhang, Y.; Yang, B.; Hou, J., Molecular Optimization Enables over 13% Efficiency in Organic Solar Cells. *J. Am. Chem. Soc.* **2017,** *139*, 7148-7151.

17. Xiao, Z.; Jia, X.; Li, D.; Wang, S.; Geng, X.; Liu, F.; Chen, J.; Yang, S.; Russell, T. P.; Ding, L., 26 mA cm^{-2} Jsc from Organic Solar Cells with A Low-bandgap Nonfullerene Acceptor. *Sci. Bull.* **2017,** *62*, 1494-1496.

18. He, Z.; Xiao, B.; Liu, F.; Wu, H.; Yang, Y.; Xiao, S.; Wang, C.; Russell, T. P.; Cao, Y., Single-Junction Polymer Solar Cells with High Efficiency and Photovoltage. *Nat. Photonics* **2015,** *9*, 174-179.

19. Huo, L.; Liu, T.; Sun, X.; Cai, Y.; Heeger, A. J.; Sun, Y., Single-junction Organic Solar Cells Based on a Novel Wide-Bandgap Polymer with Efficiency of 9.7%. *Adv. Mater.* **2015,** *27*, 2938-2944.

20. Liu, Y.; Zhao, J.; Li, Z.; Mu, C.; Ma, W.; Hu, H.; Jiang, K.; Lin, H.; Ade, H.; Yan, H., Aggregation and Morphology Control Enables Multiple Cases of High-efficiency Polymer Solar Cells. *Nat. Commun.* **2014,** *5*, 5293 (1-8).

21. Nam, S.; Song, M.; Kim, H.; Bradley, D. D.; Kim, Y., Thickness Effect of Bulk Heterojunction Layers on the Performance and Stability of Polymer: Fullerene Solar Cells with Alkylthiothiophene-containing Polymer. *ACS Sustainable Chem. Eng.* **2017,** *5*, 9263-9270.

22. Vohra, V.; Kawashima, K.; Kakara, T.; Koganezawa, T.; Osaka, I.; Takimiya, K.; Murata, H., Efficient Inverted Polymer Solar Cells Employing Favourable Molecular Orientation. *Nat. Photonics* **2015,** *9*, 403-408.

23. Zhao, J.; Li, Y.; Yang, G.; Jiang, K.; Lin, H.; Ade, H.; Ma, W.; Yan, H., Efficient Organic Solar Cells Processed from Hydrocarbon Solvents. *Nat. Energy* **2016,** *1*, 15027 (1-7).

24. Lingxia Meng, Y. Z., Xiangjian Wan, Chenxi Li, Xin Zhang, Yanbo Wang, Xin Ke, Zuo Xiao, Liming Ding, Ruoxi Xia, Hin-Lap Yip, Yong Cao, Yongsheng Chen, Organic and Solution-Processed Tandem Solar Cells with 17.3% Efficiency. *Science* **2018**, 361, 1094-1098.

25. Che, X. Z.; Li, Y. X.; Qu, Y.; Forrest, S. R., High Fabrication Yield Organic Tandem Photovoltaics Combining Vacuum- and Solution-Processed Subcells with 15% Efficiency. *Nat Energy* **2018,** *3*, 422-427.

26. Xiao, Z.; Jia, X.; Ding, L., Ternary Organic Solar Cells Offer 14% Power Conversion Efficiency. *Sci. Bull* **2017,** *62*, 1562-1564.

27. Eastham, N. D.; Dudnik, A. S.; Harutyunyan, B.; Aldrich, T. J.; Leonardi, M. J.;

Manley, E. F.; Butler, M. R.; Harschneck, T.; Ratner, M. A.; Chen, L. X., Enhanced Light Absorption in Fluorinated Ternary Small-Molecule Photovoltaics. *ACS Energy Lett.* **2017,** *2*, 1690-1697.

28. Farahat, M. E.; Patra, D.; Lee, C.-H.; Chu, C.-W., Synergistic Effects of Morphological Control and Complementary Absorption in Efficient All-Small-Molecule Ternary-Blend Solar Cells. *ACS Appl. Mater. Interfaces* **2015,** *7*, 22542-22550.

29. Huang, T.-Y.; Patra, D.; Hsiao, Y.-S.; Chang, S. H.; Wu, C.-G.; Ho, K.-C.; Chu, C.-W., Efficient Ternary Bulk Heterojunction Solar Cells based on Small Molecules Only. *J. Mater. Chem. A* **2015,** *3*, 10512-10518.

30. Zhang, M.; Zhang, F.; An, Q.; Sun, Q.; Wang, W.; Ma, X.; Zhang, J.; Tang, W., Nematic Liquid Crystal Materials as A Morphology Regulator for Ternary Small Molecule Solar Cells with Power Conversion Efficiency Exceeding 10%. *J. Mater. Chem. A* **2017,** *5*, 3589-3598.

31. Li, H.; Xiao, Z.; Ding, L.; Wang, J., Thermostable Single-Junction Organic Solar Cells with A Power Conversion Efficiency of 14.62%. *Sci. Bull* **2018,** *63*, 340-342.

32. Kan, B.; Feng, H.; Wan, X.; Liu, F.; Ke, X.; Wang, Y.; Wang, Y.; Zhang, H.; Li, C.; Hou, J., Small-Molecule Acceptor based on the Heptacyclic Benzodi (cyclopentadithiophene) Unit for Highly Efficient Nonfullerene Oganic Solar Cells. *J. Am. Chem. Soc.* **2017,** *139*, 4929-4934.

33. Yang, L.; Zhang, S.; He, C.; Zhang, J.; Yao, H.; Yang, Y.; Zhang, Y.; Zhao, W.; Hou, J., New Wide Band Gap Donor for Efficient Fullerene-Free All-small-molecule Organic Solar Cells. *J. Am. Chem. Soc.* **2017,** *139*, 1958-1966.

34. Zhou, J.; Zuo, Y.; Wan, X.; Long, G.; Zhang, Q.; Ni, W.; Liu, Y.; Li, Z.; He, G.; Li, C., Solution-processed and High-performance Organic Solar Cells Using Small Molecules with A Benzodithiophene Unit. *J. Am. Chem. Soc.* **2013,** *135*, 8484-8487.

35. Meng, L.; Zhang, Y.; Wan, X.; Li, C.; Zhang, X.; Wang, Y.; Ke, X.; Xiao, Z.; Ding, L.; Xia, R., Organic and Solution-Processed Tandem Solar Cells with 17.3% Efficiency. *Science* **2018,** *361*, 1094-1098.

36. Nian, L.; Gao, K.; Jiang, Y.; Rong, Q.; Hu, X.; Yuan, D.; Liu, F.; Peng, X.; Russell, T. P.; Zhou, G., Small-Molecule Solar Cells with Simultaneously Enhanced Short-Circuit Current and Fill Factor to Achieve 11% Efficiency. *Adv. Mater.* **2017,** *29*,

1700616 (1-7).

37. Xiao, L. G.; Chen, S.; Gao, K.; Peng, X. B.; Liu, F.; Cao, Y.; Wong, W. Y.; Wong, W. K.; Zhu, X. J., New Terthiophene-Conjugated Porphyrin Donors for Highly Efficient Organic Solar Cells. *ACS Appl. Mater. Interfaces* **2016,** *8*, 30176-30183.

38. Wang, H. D.; Xiao, L. G.; Yan, L.; Chen, S.; Zhu, X. J.; Peng, X. B.; Wang, X. Z.; Wong, W. K.; Wong, W. Y., Structural Engineering of Porphyrin-based Small Molecules as Donors for Efficient Organic Solar Cells. *Chem. Sci.* **2016,** *7*, 4301-4307.

39. Chen, S.; Xiao, L. G.; Zhu, X. J.; Peng, X. B.; Wong, W. K.; Wong, W. Y., Solution-Processed new Porphyrin-based Small Molecules as Electron Donors for Highly Efficient Organic Photovoltaics. *Chem. Commun* **2015,** *51*, 14439-14442.

40. Gao, K.; Li, L. S.; Lai, T. Q.; Xiao, L. G.; Huang, Y.; Huang, F.; Peng, J. B.; Cao, Y.; Liu, F.; Russell, T. P.; Janssen, R. A. J.; Peng, X. B., Deep Absorbing Porphyrin Small Molecule for High-Performance Organic Solar Cells with Very Low Energy Losses. *J. Am. Chem. Soc.* **2015,** *137*, 7282-7285.

41. Qin, H. M.; Li, L. S.; Guo, F. Q.; Su, S. J.; Peng, J. B.; Cao, Y.; Peng, X. B., Solution-processed Bulk Heterojunction Solar Cells based on a Porphyrin Small Molecule with 7% Power Conversion Efficiency. *Energ. Environ. Sci.* **2014,** *7*, 1397-1401.

42. Arrechea, S.; Aljarilla, A.; de la Cruz, P.; Singh, M. K.; Sharma, G. D.; Langa, F., New Cyclopentadithiophene (CDT) Linked Porphyrin Donors with Different End-capping Acceptors for Efficient Small Molecule Organic Solar Cells. *J. Mater. Chem. C* **2017,** *5*, 4742-4751.

43. Mishra, R.; Regar, R.; Singhal, R.; Panini, P.; Sharma, G. D.; Sankar, J., Porphyrin based Push-Pull Conjugates as Donors for Solution-Processed Bulk Heterojunction Solar Cells: A case of Metal-Dependent Power Conversion Efficiency. *J. Mater. Chem. A* **2017,** *5*, 15529-15533.

44. Xiao, Z.; Yang, S.; Yang, Z.; Yang, J.; Yip, H. L.; Zhang, F.; He, F.; Wang, T.; Wang, J.; Yuan, Y., Carbon–Oxygen-Bridged Ladder-Type Building Blocks for Highly Efficient Nonfullerene Acceptors. *Adv. Mater.* **2018**, 1804790 (1-6).

45. Chen, S.; Yan, L.; Xiao, L. G.; Gao, K.; Tang, W.; Wang, C.; Zhu, C. H.; Wang, X. Z.; Liu, F.; Peng, X. B.; Wong, W. K.; Zhu, X. J., A Visible-Near-Infrared Absorbing A-π(2)-D-π(1)-D-π(2)-A Type Dimeric-Porphyrin Donor for High-Performance Organic Solar

Cells. *J. Mater. Chem. A* **2017,** *5*, 25460-25468.

46. Nian, L.; Gao, K.; Liu, F.; Kan, Y. Y.; Jiang, X. F.; Liu, L. L.; Xie, Z. Q.; Peng, X. B.; Russell, T. P.; Ma, Y. G., 11% Efficient Ternary Organic Solar Cells with High Composition Tolerance via Integrated Near-IR Sensitization and Interface Engineering. *Adv. Mater.* **2016,** *28*, 8184-8190.

47. Zhou, L.; Xu, Z.-X.; Zhou, Y.; Feng, Y.; Zhou, X.-G.; Xiang, H.-F.; Roy, V., Structure–Charge Transport Relationship of 5, 15-Dialkylated Porphyrins. *Chem. Commun.* **2012,** *48*, 5139-5141.

48. Wang, Z.; Xu, X.; Li, Z.; Feng, K.; Li, K.; Li, Y.; Peng, Q., Solution-Processed Organic Solar Cells with 9.8% Efficiency Based on a New Small Molecule Containing a 2D Fluorinated Benzodithiophene Central Unit. *Adv. Electronic Mater.* **2016,** *2*, 1600061(1-7).

49. Cuesta, V.; Vartanian, M.; de la Cruz, P.; Singhal, R.; Sharma, G. D.; Langa, F., Comparative Study on the Photovoltaic Characteristics of A-D-A and D-A-D Molecules based on Zn-Porphyrin; a D-A-D Molecule with Over 8.0% Efficiency. *J. Mater. Chem. A* **2017,** *5*, 1057-1065.

50. Kumar, C. V.; Cabau, L.; Koukaras, E. N.; Sharma, A.; Sharma, G. D.; Palomares, E., A-π-D-π-A based Porphyrin for Solution Processed Small Molecule Bulk Heterojunction Solar Cells. *J. Mater. Chem. A* **2015,** *3*, 16287-16301.

51. Lin, V.; DiMagno, S. G.; Therien, M. J., Highly Conjugated, Acetylenyl Bridged Porphyrins: New Models for Light-Harvesting Antenna Systems. *Science* **1994,** *264*, 1105-1111.

52. Schmitt, J.; Heitz, V.; Jenni, S.; Sour, A.; Bolze, F.; Ventura, B., π-Extended Porphyrin Dimers as Efficient Near-Infrared Emitters and Two-Photon Absorbers. *Supramol. Chem.* **2017,** *29* , 769-775.

53. Ariu, M.; Sims, M.; Rahn, M.; Hill, J.; Fox, A.; Lidzey, D.; Oda, M.; Cabanillas-Gonzalez, J.; Bradley, D., Exciton Migration in β-phase Poly (9, 9-dioctylfluorene). *Phy. Rev. B* **2003,** *67*, 195333 (1-11).

54. Xiao, L.; Liang, T.; Gao, K.; Lai, T.; Chen, X.; Liu, F.; Russell, T. P.; Huang, F.; Peng, X.; Cao, Y., Ternary Solar Cells based on Two Small Molecule Donors with Same Conjugated Backbone: the Role of Good Miscibility and Hole Relay Process. *ACS Appl. Mater. Interfaces* **2017,** *9*, 29917-29923.

55. Nian, L.; Gao, K.; Liu, F.; Kan, Y.; Jiang, X.; Liu, L.; Xie, Z.; Peng, X.; Russell, T. P.; Ma, Y., 11% Efficient Ternary Organic Solar Cells with High Composition Tolerance via Integrated Near-IR Sensitization and Interface Engineering. *Adv. Mater.* **2016,** *28*, 8184-8190.

56. Kan, B.; Yi, Y. Q. Q.; Wan, X.; Feng, H.; Ke, X.; Wang, Y.; Li, C.; Chen, Y., Ternary Organic Solar Cells With 12.8% Efficiency Using Two Nonfullerene Acceptors With Complementary Absorptions. *Adv. Energy Mater.* **2018**, 1800424 (1-7).

57. Kyaw, A. K. K.; Wang, D. H.; Gupta, V.; Leong, W. L.; Ke, L.; Bazan, G. C.; Heeger, A. J., Intensity Dependence of Current–Voltage Characteristics and Recombination in High-Efficiency Solution-Processed Small-Molecule Solar Cells. *ACS nano* **2013,** *7*, 4569-4577.

58. Kyaw, A. K. K.; Wang, D. H.; Wynands, D.; Zhang, J.; Nguyen, T.-Q.; Bazan, G. C.; Heeger, A. J., Improved Light Harvesting and Improved Efficiency by Insertion of An Optical Spacer (ZnO) in Solution-Processed Small-Molecule Solar Cells. *Nano Lett.* **2013,** *13*, 3796-3801.

59. Lu, L.; Chen, W.; Xu, T.; Yu, L., High-Performance Ternary Blend Polymer Solar Cells Involving both Energy Eransfer and Hole Relay Processes. *Nat. Commun.* **2015,** *6*, 7327 (1-7).

60. Min, J.; Jiao, X.; Ata, I.; Osvet, A.; Ameri, T.; Bäuerle, P.; Ade, H.; Brabec, C. J., Time-Dependent Morphology Evolution of Solution-Processed Small Molecule Solar Cells during Solvent Vapor Annealing. *Adv. Energy Mater.* **2016,** *6*, 1502579 (1-9).

61. Riedel, I.; Parisi, J.; Dyakonov, V.; Lutsen, L.; Vanderzande, D.; Hummelen, J. C., Effect of Temperature and Illumination on the Electrical Characteristics of Polymer–Fullerene Bulk-Heterojunction Solar Cells. *Adv. Funct. Mater.* **2004,** *14*, 38-44.

62. Ma, X.; Gao, W.; Yu, J.; An, Q.; Zhang, M.; Hu, Z.; Wang, J.; Tang, W.; Yang, C.; Zhang, F., Ternary Nonfullerene Polymer Solar Cells with Efficiency> 13.7% by Integrating the Advantages of Materials and Two Binary Cells. *Energy Environ. Sci.* **2018,** *11*, 2134-2141.

TOC Graphic

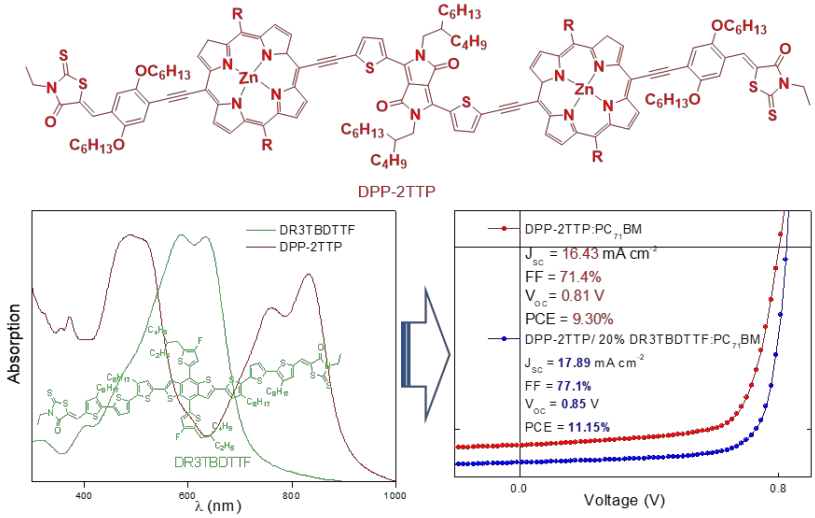
DPP-2TTP
DR3TBDTTF
DPP-2TTP
Absorption
λ (nm)
DPP-2TTP:PC71BM
JSC = 16.43 mA cm-2
FF = 71.4%
VOC = 0.81 V
PCE = 9.30%
DPP-2TTP/ 20% DR3TBDTTF:PC71BM
JSC = 17.89 mA cm-2
FF = 77.1%
VOC = 0.85 V
PCE = 11.15%
Current Density (mA cm-2)
Voltage (V)